The Astrophysical Journal, 756:160 (8pp), 2012 September 10 doi:10.1088/0004-637X/756/2/160

CONSTRAINTS ON THE FAINT END OF THE QUASAR LUMINOSITY FUNCTION AT $z \sim 5$ IN THE COSMOS FIELD

H. Ikeda[1,2], T. Nagao[2,3], K. Matsuoka[1,2,13], Y. Taniguchi[4], Y. Shioya[4], M. Kajisawa[1,4], M. Enoki[5], P. Capak[6], F. Civano[7], A. M. Koekemoer[8], D. Masters[6,9], T. Morokuma[10], M. Salvato[11], E. Schinnerer[12], and N. Z. Scoville[6]

[1] Graduate School of Science and Engineering, Ehime University, Bunkyo-cho, Matsuyama 790-8577, Japan; ikeda@cosmos.phys.sci.ehime-u.ac.jp
[2] Department of Astronomy, Graduate School of Science, Kyoto University, Kitashirakawa-Oiwake-cho, Sakyo-ku, Kyoto 606-8502, Japan
[3] The Hakubi Center for Advanced Research, Kyoto University, Yoshida-Ushinomiya-cho, Sakyo-ku, Kyoto 606-8302, Japan
[4] Research Center for Space and Cosmic Evolution, Ehime University, Bunkyo-cho, Matsuyama 790-8577, Japan
[5] Faculty of Business Administration, Tokyo Keizai University, 1-7-34 Minami-cho, Kokubunji, Tokyo 185-8502, Japan
[6] Department of Astronomy, 249-17 Caltech, 1201 East California Boulevard, Pasadena, CA 91125, USA
[7] Harvard Smithsonian Center for Astrophysics, 60 Garden Street, Cambridge, MA 02138, USA
[8] Space Telescope Science Institute, 3700 San Martin Drive, Baltimore, MD 21218, USA
[9] Department of Physics and Astronomy, University of California, 900 University Avenue, Riverside, CA 92521, USA
[10] Institute of Astronomy, Graduate School of Science, University of Tokyo, 2-21-1 Osawa, Mitaka 181-0015, Japan
[11] Max-Planck-Institut für Plasmaphysik, Boltzmanstrasse 2, D-85741 Garching, Germany
[12] Max-Planck-Institut für Astronomie, Königstuhl 17, D-69117 Heidelberg, Germany

Received 2011 July 9; accepted 2012 July 6; published 2012 August 24

ABSTRACT

We present the result of our low-luminosity quasar survey in the redshift range of $4.5 \lesssim z \lesssim 5.5$ in the COSMOS field. Using the COSMOS photometric catalog, we selected 15 quasar candidates with $22 < i' < 24$ at $z \sim 5$ that are ~3 mag fainter than the Sloan Digital Sky Survey quasars in the same redshift range. We obtained optical spectra for 14 of the 15 candidates using FOCAS on the Subaru Telescope and did not identify any low-luminosity type-1 quasars at $z \sim 5$, while a low-luminosity type-2 quasar at $z \sim 5.07$ was discovered. In order to constrain the faint end of the quasar luminosity function at $z \sim 5$, we calculated the 1σ confidence upper limits of the space density of type-1 quasars. As a result, the 1σ confidence upper limits on the quasar space density are $\Phi < 1.33 \times 10^{-7}$ Mpc^{-3} mag^{-1} for $-24.52 < M_{1450} < -23.52$ and $\Phi < 2.88 \times 10^{-7}$ Mpc^{-3} mag^{-1} for $-23.52 < M_{1450} < -22.52$. The inferred 1σ confidence upper limits of the space density are then used to provide constraints on the faint-end slope and the break absolute magnitude of the quasar luminosity function at $z \sim 5$. We find that the quasar space density decreases gradually as a function of redshift at low luminosity ($M_{1450} \sim -23$), being similar to the trend found for quasars with high luminosity ($M_{1450} < -26$). This result is consistent with the so-called downsizing evolution of quasars seen at lower redshifts.

Key words: cosmology: observations – quasars: general – surveys

Online-only material: color figures

1. INTRODUCTION

The evolution of supermassive black holes (SMBHs) is now regarded as one of the most important unresolved issues in the modern astronomy, after the discovery of the galaxy–SMBH "co-evolution" inferred from, e.g., a tight relationship between the mass of SMBHs and their host bulges (e.g., Marconi & Hunt 2003; Häring & Rix 2004; Gültekin et al. 2009). Measuring the whole shape of the quasar luminosity function (QLF) is particularly important to understand how the SMBHs grew, since it is highly dependent on some key parameters of SMBHs such as the growth timescale of SMBHs (e.g., Enoki et al. 2003).

The QLF at $z \lesssim 3$ has been well quantified over a wide luminosity range (e.g., Croom et al. 2009) and is best represented by a double power law (e.g., Boyle et al. 1988; Pei 1995). Recently, the faint end of the QLF at $z \sim 4$ has been measured (Glikman et al. 2010, 2011; Ikeda et al. 2011) and is also best represented by a double power law. More interestingly, recent studies on the optical QLF show that the space density of low-luminosity active galactic nuclei (AGNs) peaks at a lower redshift than that of more luminous AGNs (Croom et al. 2009; Ikeda et al. 2011). This result can be interpreted as AGN (or SMBH) downsizing evolution, since the brighter AGNs tend to harbor the more massive SMBHs if the dispersion of the Eddington ratio of quasars is not very large (see, e.g., Trump et al. 2011). The AGN downsizing has also been reported by X-ray surveys (Ueda et al. 2003; Hasinger et al. 2005; see also Brusa et al. 2009; Civano et al. 2011). However, the physical origin of the AGN downsizing is totally unclear, which makes high-z low-luminosity quasar surveys more important (see Fanidakis et al. 2012 for theoretical works on the AGN downsizing evolution).

Recently, some low-luminosity quasar surveys have been performed at $z > 5$ (Cool et al. 2006; Mahabal et al. 2005). Cool et al. (2006) identified three quasars at $z > 5$ with $z' < 22$ and included a quasar at $z = 5.85$ with $z' = 20.68$, in the AGES survey which covers 8.5 deg^2. Jiang et al. (2008) also identified five new quasars at $z > 5.8$ with $20 < z' < 21$ in the Sloan Digital Sky Survey (SDSS) deep stripe which covers 260 deg^2. The space density of quasars at $z \sim 6$, which is calculated by the result of Cool et al. (2006), is about six times larger than the result of Jiang et al. (2008). This large discrepancy may be caused by the small survey area of Cool et al. (2006). Mahabal et al. (2005) identified a very faint quasar at $z = 5.70$ with $z' = 23.0$ in the total quasar survey area of 2.5 deg^2. Mahabal et al. (2005) mentioned that the surface density of quasars at similar redshifts is roughly consistent with previous extrapolations of the faint end of the QLF. In this way, some low-luminosity

[13] Research Fellow of the Japan Society for the Promotion of Science.

quasars have been discovered although the faint end of QLF is not determined exactly, due to the lack of low-luminosity quasars.

At $z > 6$, a number of luminous quasars have been found up to $z \sim 6.5$ by the SDSS (e.g., Fan et al. 2006; Goto 2006; Jiang et al. 2008, 2009) and the Canada–France High-z Quasar Survey (CFHQS; Willott et al. 2007, 2009, 2010). Recently, a luminous quasar at $z = 7.085$ has been found (Mortlock et al. 2011) through the data obtained by the United Kingdom Infrared Telescope Infrared Deep Sky Survey (UKIDSS; Lawrence et al. 2007). Although some low-luminosity quasars at $z > 5$ have been discovered as mentioned above, the faint-end slope of the $z > 5$ QLF is still very poorly constrained. Consequently, it is not understood how low-luminosity quasars evolve at high redshifts, or if the AGN downsizing evolution is also seen in the earlier universe. Since the number density of low-luminosity quasars is expected to be much higher than that of high-luminosity quasars, the whole picture of SMBH evolution cannot be understood without firm measurements of the number density of low-luminosity quasars at such high redshifts.

Motivated by these issues, we have searched for low-luminosity quasars at $z \sim 5$ in the COSMOS field (Scoville et al. 2007). In Section 2, we describe the data and method that were used for the photometric selection of quasar candidates. In Section 3, we report the results of the follow-up spectroscopic observations. In Section 4, we describe how we estimate the photometric completeness to derive the QLF. In Section 5, we present the upper limits of the QLF at $z \sim 5$ and briefly discuss it. Throughout this paper, we use a Λ cosmology with $\Omega_m = 0.3$, $\Omega_\Lambda = 0.7$, and the Hubble constant of $H_0 = 70$ km s^{-1} Mpc^{-1}.

2. THE SAMPLE

2.1. The Cosmic Evolution Survey

The COSMOS is a treasury program on the *Hubble Space Telescope* (*HST*) and comprises 270 and 320 orbits allocated with *HST* Cycles 12 and 13, respectively (Scoville et al. 2007; Koekemoer et al. 2007). The COSMOS field covers an area of $1.^\circ4 \times 1.^\circ4$ square which corresponds to 2 deg^2, centered at R.A. (J2000) = 10:00:28.6 and decl. (J2000) = +02:12:21.0.

We use the official COSMOS photometric redshift catalog for photometry (Ilbert et al. 2009; see also Capak et al. 2007) to select the quasar photometric candidates at $z \sim 5$. This catalog covers an area of $\sim$2 deg^2 and contains several photometric measurements. Specifically, in this paper we use the u^*-band 3″ diameter aperture apparent magnitude measured on the image obtained with MegaCam (Boulade et al. 2003) on the Canada–France–Hawaii Telescope (CFHT), and the 3″ diameter aperture apparent magnitudes of the g', r', i', and z' bands (Taniguchi et al. 2007) measured on the image obtained with the Subaru Suprime-Cam (Miyazaki et al. 2002), and the i'-band total apparent magnitude (MAG_AUTO measured by SExtractor; Bertin & Arnouts 1996) whose measurement is also based on the Suprime-Cam i'-band image.

The 5σ limiting AB apparent magnitudes are $u^* = 26.5$, $g' = 26.5$, $r' = 26.6$, $i' = 26.1$, and $z' = 25.1$ (3″ diameter aperture). Since we also use the Advanced Camera for Surveys (ACS) catalog (Koekemoer et al. 2007; Leauthaud et al. 2007) to separate galaxies from point sources, our survey area is restricted to the area mapped with ACS on *HST* (1.64 deg^2). Note that all of the data in the official COSMOS photometric redshift catalog overlap the entire ACS field.

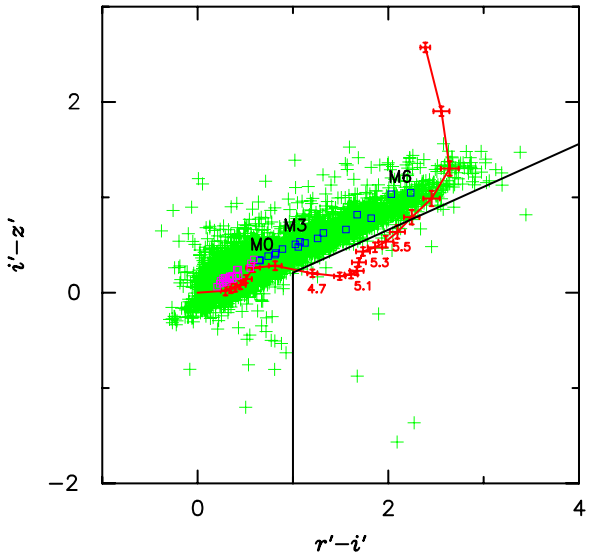

Figure 1. Two-color diagram of $r' - i'$ and $i' - z'$ that is used for our quasar selection. Green plus signs denote point sources with $22 < i'$(MAG_AUTO) < 24. Blue and magenta squares denote colors of M- and K-type stars (Pickles 1998), respectively. The red line is the median track of the model quasar colors. The red error bars show the standard deviation of the $r' - i'$ and $i' - z'$ colors in our model quasar spectra. The black solid line shows our photometric criteria used to select quasar candidates at $z \sim 5$.

(A color version of this figure is available in the online journal.)

2.2. Quasar Candidate Selection

Quasars at $z \sim 5$ show the Lyman break in their spectral energy distribution (SED) that falls between the wavelengths of the r' and i' filters, making their $r' - i'$ color redder than their $i' - z'$ color. We utilize this property to select candidates of low-luminosity quasars at $z \sim 5$. Here, typical quasar colors as a function of redshift are necessary to define reliable color-selection criteria for quasars at $z \sim 5$. Therefore, we generate model quasar spectra following the procedure generally adopted in previous studies (e.g., Fan 1999; Hunt et al. 2004; Richards et al. 2006; Siana et al. 2008), and derive the $g' - r'$, $r' - i'$, and $i' - z'$ colors of the model quasars at redshifts from 0 to 6. In this procedure, we adopt the typical power-law slope ($\alpha_\nu = 0.46$, where $f_\nu \propto \nu^{-\alpha_\nu}$), Ly$\alpha$ rest-frame equivalent width (EW$_0$ = 90 Å), and typical emission-line flux ratios (Vanden Berk et al. 2001). The effects of the intergalactic absorption by the neutral hydrogen were corrected by adopting the extinction model of Madau (1995). Our simulated colors of the model quasars are shown in the $r' - i'$ versus $i' - z'$ diagram (Figure 1). Note that the dispersions in the power-law slope and EWs of quasars are also taken into account when we calculate the photometric completeness of our survey (see Section 4).

We select our quasar photometric candidates at $z \sim 5$ using the following criteria:

$$22 < i'(\mathrm{MAG\_AUTO}) < 24, \quad (1)$$

$$i' - z' < 0.45(r' - i') - 0.24, \quad (2)$$

$$u^* > 27.49, \quad (3)$$

$$g' - r' \geqslant 1.3, \quad (4)$$

and

$$r' - i' > 1.0. \quad (5)$$

The criterion (2) is used to select quasars efficiently without significant contamination from stars (especially from M0 to M6; see also Figure 1), taking the color distribution of stars and model quasars into account. To remove possible foreground contaminations further, we introduce the additional criteria (3), (4), and (5). These latter two-color thresholds are adopted by taking empirical color distributions of quasars at $z \sim 5$ into account (Richards et al. 2006).

Here we comment on our point-source criterion based on the *HST* image ($F814W$; see Koekemoer et al. 2007), whose spatial resolution is 0.″09 in FWHM (which corresponds to ∼0.6 kpc at $z = 5$). Since the size of high-z quasar host galaxies is larger than 1 kpc (Targett et al. 2012), it is expected that the quasar host galaxies are spatially resolved in the ACS images. Therefore, it would be possible that some quasars could be excluded from the sample of our quasar photometric candidates. However, at $z \sim 1$, some earlier works show that the host galaxy of quasars with a similar absolute magnitude to our targets is typically ∼2 mag fainter than their nucleus (e.g., McLeod & McLeod 2001; McLeod & Bechtold 2009). The brightness difference may be even larger at higher redshifts because the typical Eddington ratio of luminous quasars is roughly constant at $z \sim 1$–4 (Trump et al. 2009) while the mass ratio of SMBHs to host galaxies is higher at higher redshifts (e.g., Treu et al. 2006; Woo et al. 2008, 2006; Merloni et al. 2010; Bennert et al. 2010, 2011). Therefore, we conclude that quasars explored in this work should be recognized as point sources in the *HST* image. To distinguish the galaxies and point sources, Leauthaud et al. (2007) used the SExtractor parameters MU_MAX (peak surface brightness above the background level) and MAG_AUTO (see Figure 5 of Leauthaud et al. 2007) because of the fact that the light distribution of a point source varies with magnitude. Therefore, we can distinguish the extended objects and point sources by using the MU_MAX and MAG_AUTO.

Accordingly, we removed 23 spatially extended objects satisfying the criteria (1)–(5) based on the classification by Leauthaud et al. (2007). As a result, we obtain a sample of 15 quasar candidates among 7318 point sources with $22 < i'$ (MAG_AUTO) < 24. The selected candidates are listed in Table 1.

Table 1
Properties of the Quasar Candidates at $z \sim 5$

Number	R.A. (deg)	Decl. (deg)	i' (MAG_AUTO) (mag)	$r' - i'$ (mag)	$i' - z'$ (mag)	Exp. Time[a] (s)
1	150.69131	1.637161	23.40	2.34	0.67	2400
2	150.45275	1.669653	23.48	2.04	2.69	3000
3	150.17448	1.629074	23.76	1.67	2.11	1800
4[b]	150.64917	1.816186	23.39	3.44	0.82	...
5	149.87082	1.882791	23.98	1.26	0.17	2400
6	149.85403	1.823611	23.97	2.58	0.87	2400
7	149.78245	2.221621	23.96	3.19	1.13	1800
8	149.69804	2.283260	23.67	2.04	0.44	1800
9	150.56861	2.317432	23.98	4.09	1.26	1800
10	150.05481	2.376726	23.89	1.09	0.25	2700
11[c]	149.78381	2.452135	23.70	1.35	0.26	7200
12	150.16401	2.549605	23.31	1.96	0.61	2400
13	149.96443	2.473646	23.93	1.21	0.21	2700
14	150.66035	2.786445	23.51	1.93	0.57	2400
15	149.59161	2.659749	23.16	2.26	0.77	2400

Notes.
[a] Total on-source exposure time in the FOCAS spectroscopic observation.
[b] This quasar candidate was not observed.
[c] Type-2 quasar at $z = 5.07$.

3. SPECTROSCOPIC OBSERVATION

The spectroscopic follow-up observations of the quasar candidates were carried out at the Subaru Telescope with the Faint Object Camera and Spectrograph (FOCAS; Kashikawa et al. 2002) on 2010 January 7–11. We used the 300 grating with the SO58 filter, whose wavelength coverage is $5800\,\text{Å} \leqslant \lambda_{\rm obs} \leqslant 10000\,\text{Å}$. We used a 0.″8 width slit, resulting in a wavelength resolution of $R \sim 700$ ($\Delta v \sim 430\,\text{km s}^{-1}$) as measured by night sky emission lines. The typical seeing size was ∼0.″7. Due to the limited observing time, we observed 14 of the 15 candidates; object No. 4 in Table 1 was not observed. The individual exposure time was 600–900 s, and the total exposure time was 1800–7200 s for each object.

Standard data reduction procedures were performed by using IRAF. After the sky subtraction, we extracted one-dimensional spectra with an aperture size of 1.″8 and the relative sensitivity calibration was performed using the spectral data of a spectrophotometric standard star, Feige 34. The spectra of 14 objects were then flux-calibrated using the i'-band photometric magnitude of these objects. We found that one spectrum shows only narrow Lyα emission lines at $\lambda_{\rm obs} = 7381\,\text{Å}$ ($z \sim 5.07$ and $\Delta v_{\rm FWHM} \sim 800\,\text{km s}^{-1}$) without any high-ionization lines such as C IV (Figure 2). Since this object is detected in the X-ray band by the *Chandra*-COSMOS survey (CID-2220; Elvis et al. 2009) and its X-ray luminosity is $3\times10^{44}\,\text{erg s}^{-1}$ in the 2–10 keV rest-frame band (Civano et al. 2011, 2012), it can be classified as an AGN. We can classify this object as a type-2 AGN based on the upper limit available for the X-ray hardness ratio consistent with mild obscuration ($N_{\rm H} < 5\times10^{23}\,\text{cm}^{-2}$) together with its Ly$\alpha$ spectral profile. Although the X-ray hardness ratio is not available for this object, we classify this object as a type-2 AGN based on its Lyα spectral profile. Therefore, we conclude that no type-1 quasars are identified in our spectroscopic follow-up campaign. The spectra of the remaining 13 objects are consistent with those of Galactic late-type stars, and an example of these spectra is shown in Figure 3.

4. COMPLETENESS

Quasar surveys are generally not perfectly complete due to various factors such as photometric errors and intrinsic variations in the spectra. Therefore, to derive the QLF accurately, the survey completeness needs to be estimated as a function of the quasar redshift and apparent magnitude. We derive the completeness by modeling quasar spectra, in a similar way as described in Section 2.2. Here we also take into account the intrinsic variation in the continuum slope and EWs of the emission lines. We assume a Gaussian distribution of the power-law slope α_ν ($f_\nu \propto \nu^{-\alpha_\nu}$) and Ly$\alpha$ EWs, with means of 0.46 and 90 Å (the same as those in Section 2.2), and a standard deviation of 0.30 and 20 Å, respectively (Vanden Berk et al. 2001; Francis 1996; Hunt et al. 2004; Glikman et al. 2010). We include emission lines whose flux is larger than 0.5% of the Lyα flux, given in Table 2 of Vanden Berk et al. (2001). The emission-line ratios are assumed to be the same for all model quasars (i.e., scaling to the Lyα strength). We also include the Balmer continuum and Fe II features by using the template of Kawara et al. (1996). We create 1000 quasar spectra at each $\Delta z = 0.01$ in the redshift range of $0 < z < 6$. The effects of intergalactic absorption by neutral hydrogen were corrected by adopting the extinction model of Madau (1995). Then, we calculated the

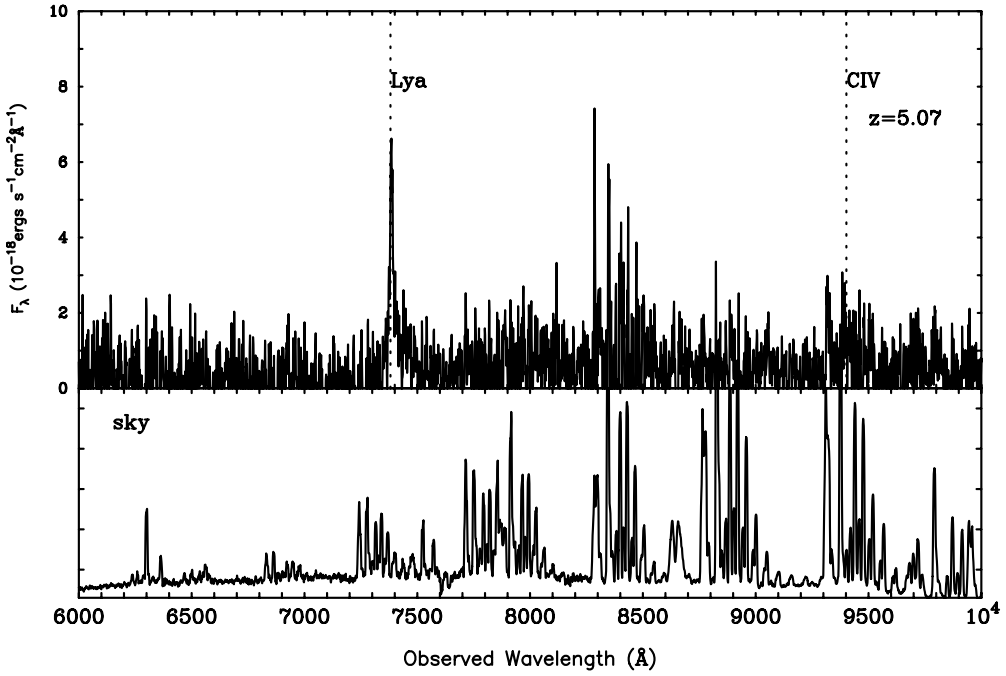

Figure 2. Reduced spectrum of object No. 11 in Table 1 (upper panel) and typical sky spectrum (lower panel). The dotted lines show the expected wavelengths of quasar emission lines: Lyα λ1216 and C IV λ1549.

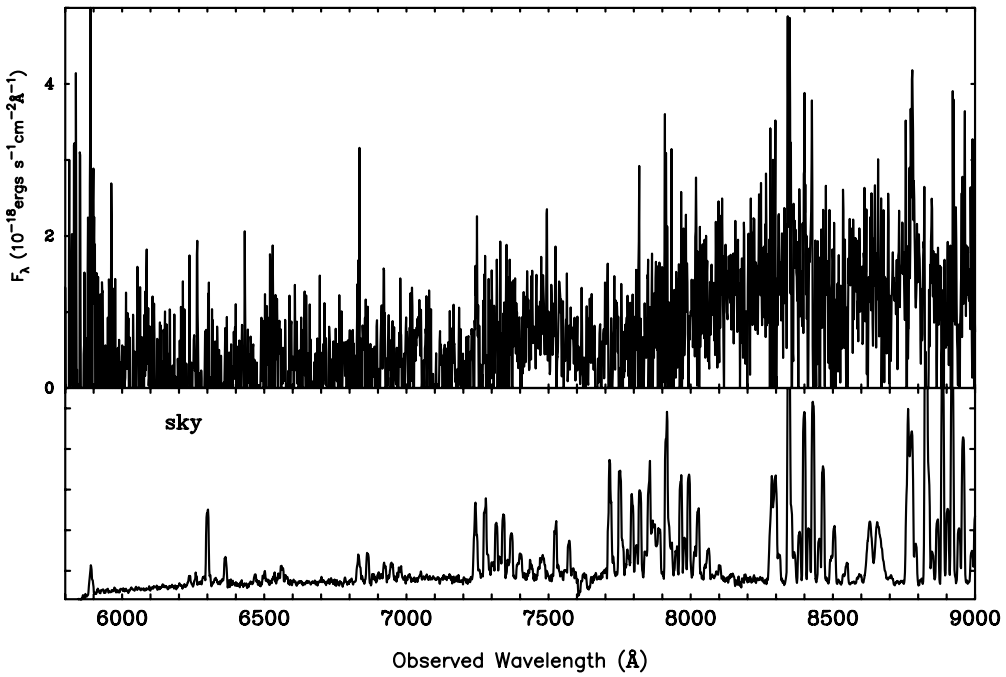

Figure 3. Example of the late-type star spectrum (upper panel; No. 2 in Table 1) and typical sky spectrum (lower panel).

colors of the model quasars in the observed frame. We compared the colors of the simulated quasars with the empirical quasar colors (SDSS DR7) to check whether the simulated quasar colors are consistent with the empirical quasar colors. Figure 4 shows the comparison between the empirical and simulated quasar colors of $g^* - r^*$, $r^* - i^*$, and $i^* - z^*$ by using the transmission curves of the SDSS filters. Note that the dispersion of the simulated quasar colors is systematically smaller than the dispersion of the observed quasar colors, though the average color is consistent between the simulated and observed quasar colors. This is because the simulated colors presented here do not take photometric errors into account. The photometric errors are properly taken into account when the completeness is calculated, as described below.

To estimate the photometric completeness, we put the 1000 model quasars at each grid point in apparent magnitude and redshift into Subaru Suprime-Cam FITS images as point sources, using the IRAF `mkobjects` task in the `artdata` package. As for 1000 model quasars, they were generated on a Monte Carlo method of drawing a value of α and EW. These point sources have apparent magnitudes calculated from their simulated spectra, in each image (g', r', i', and z'). We then tried to detect

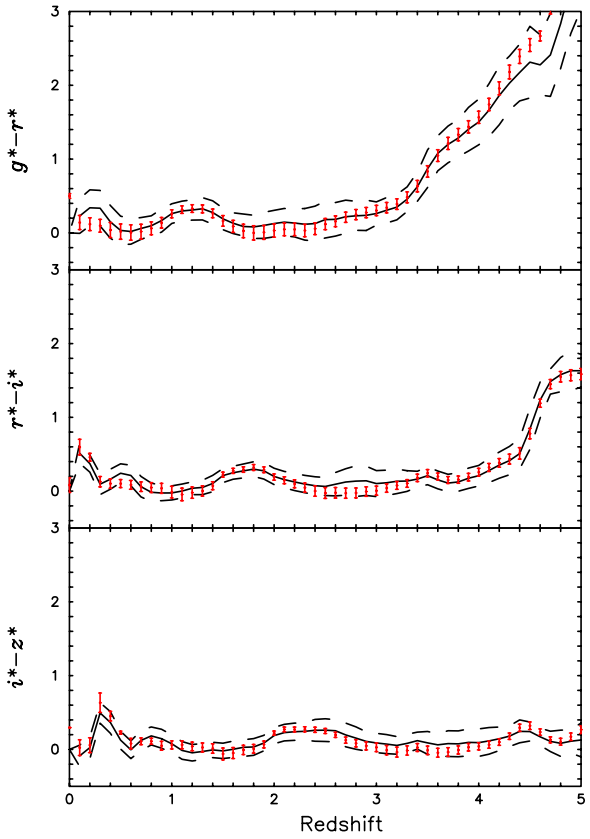

Figure 4. Comparison between the empirical and simulated quasar colors. Solid black lines show the empirical mean colors of the SDSS DR7 quasars. Dashed black lines show 1σ dispersions of the SDSS DR7 quasar colors. Red points show the simulated quasar colors. Red vertical lines show the standard deviation of simulated quasar colors, which do not include photometric errors.

(A color version of this figure is available in the online journal.)

them in the i'-band image with SExtractor, and measure their colors in the double-image mode. Note that the measured apparent magnitudes and colors of the simulated quasars are generally different from the magnitudes and colors before inserted into the Suprime-Cam images, due to the effects of photometric errors and neighboring foreground objects. Accordingly, some model quasars are not selected as photometric candidates of quasar with the criteria (1)–(5). To calculate the fraction of model quasars that are selected as photometric candidates in the above process, we estimate the photometric completeness at various magnitudes and redshifts (Figure 5). The redshift range of the inferred completeness is moderately high at $4.5 \lesssim z \lesssim 5.5$. More specifically, the inferred completeness is ~90% for quasars with $i' = 22.5$, and ~80% for those with $i' = 23.5$ in that redshift range. The small dip at $z \sim 5.2$–5.3 in the estimated completeness is due to the C IV emission that causes the $i' - z'$ color to be red at that redshift range.

5. QUASAR LUMINOSITY FUNCTION

To calculate the upper limits of the quasar space density, we compute the effective comoving volume of the survey as

$$V_{\rm eff}(m_{i'}) = d\Omega \int_{z=0}^{z=\infty} C(m_{i'}, z) \frac{dV}{dz} dz, \quad (6)$$

where $d\Omega$ is the solid angle of the survey and $C(m_{i'}, z)$ is the photometric completeness derived in Section 4. For comparison

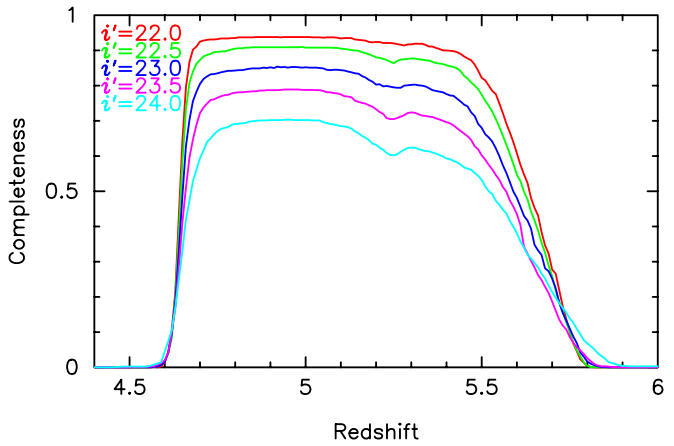

Figure 5. Simulated photometric completeness. Red, green, blue, purple, and cyan lines show the completeness for quasars with $m_{i'} = 22.0$, 22.5, 23.0, 23.5, and 24.0, respectively.

(A color version of this figure is available in the online journal.)

with other works, we convert the i'-band apparent magnitude to the absolute AB magnitude at 1450 Å (e.g., Richards et al. 2006; Croom et al. 2009; Glikman et al. 2010):

$$M_{1450} = m_{i'} + 5 - 5\log d_L(z) + 2.5(1-\alpha_\nu)\log(1+z) + 2.5\alpha_\nu \log\left(\frac{\lambda_{i'}}{1450\ \text{Å}}\right), \quad (7)$$

where $d_L(z)$, α_ν, and $\lambda_{i'}$ are the luminosity distance, spectral index of the quasar continuum ($f_\nu \propto \nu^{-\alpha_\nu}$), and the effective wavelength of the i' band ($\lambda_{i'} = 7684$ Å), respectively. We assumed $\alpha_\nu = 0.46$ when we used Equation (7). As for the quasar candidates that did not perform the spectroscopic observations, we calculated the absolute magnitude at 1450 Å by assuming the effective redshift. Given the effective comoving volume, the 1σ confidence upper limits on the space density of type-1 quasars are calculated using statistics from Gehrels (1986).

The derived 1σ confidence upper limits on the space density of type-1 quasars are $\Phi < 1.33 \times 10^{-7}$ Mpc^{-3} mag^{-1} for $-24.52 < M_{1450} < -23.52$ and $\Phi < 2.88 \times 10^{-7}$ Mpc^{-3} mag^{-1} for $-23.52 < M_{1450} < -22.52$. Note that there is another quasar candidate in the magnitude bin of $-23.52 < M_{1450} < -22.52$ which was not observed with FOCAS. We take into account the possibility that this candidate is a quasar when calculating the 1σ confidence upper limit on the space density of type-1 quasars for $-23.52 < M_{1450} < -22.52$. The obtained 1σ confidence upper limits on the space density of type-1 quasars are plotted in Figure 6.

To compare our upper limits on the quasar space density with the previous quasar surveys at similar redshifts, we also plot the results of COMBO-17 (Wolf et al. 2003), SDSS (Richards et al. 2006), and GOODS (Fontanot et al. 2007) in the redshift ranges of $4.2 < z < 4.8$, $4.5 < z < 5.0$, and $4.0 < z < 5.2$, respectively, in Figure 6. Note that the low-luminosity quasar sample of Fontanot et al. (2007) includes type-2 quasars, while our sample and the sample of Wolf et al. (2003) do not include type-2 quasars. To compare the result of Fontanot et al. (2007), we also calculated the quasar space density when we included a type-2 quasar and the obtained quasar space density and its error are $\Phi = 0.87^{+2.01}_{-0.72} \times 10^{-7}$ Mpc^{-3} mag^{-1} for $-23.52 < M_{1450} < -22.52$ (see Figure 6). This figure shows a marginal discrepancy between the results of Fontanot et al.

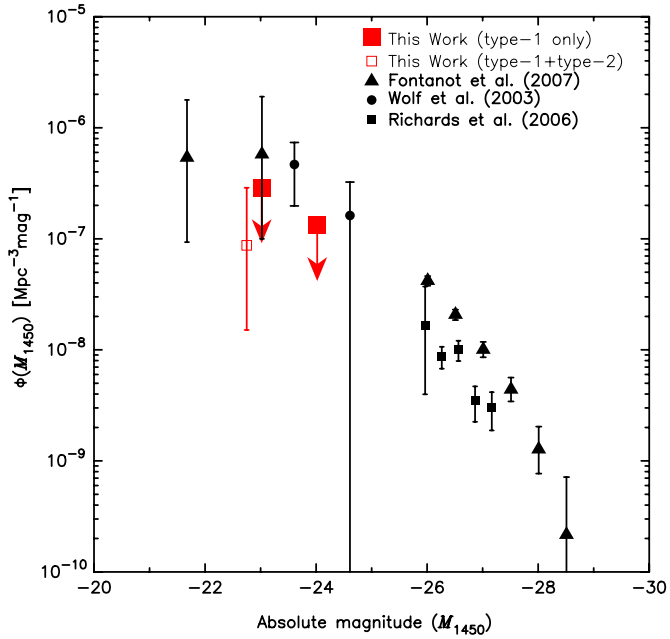

Figure 6. $z \sim 5$ quasar luminosity functions. The red filled squares show our results (1σ confidence limits on the quasar space density) and the red open square shows the quasar space density when we include a type-2 quasar at $z \sim 5.07$. For clarifying the data plots in the figure, the open red square is slightly shifted to the left direction to avoid the overlap of the error bars. Triangles, squares, and circles denote the results reported by Fontanot et al. (2007), Richards et al. (2006), and Wolf et al. (2003), respectively.

(A color version of this figure is available in the online journal.)

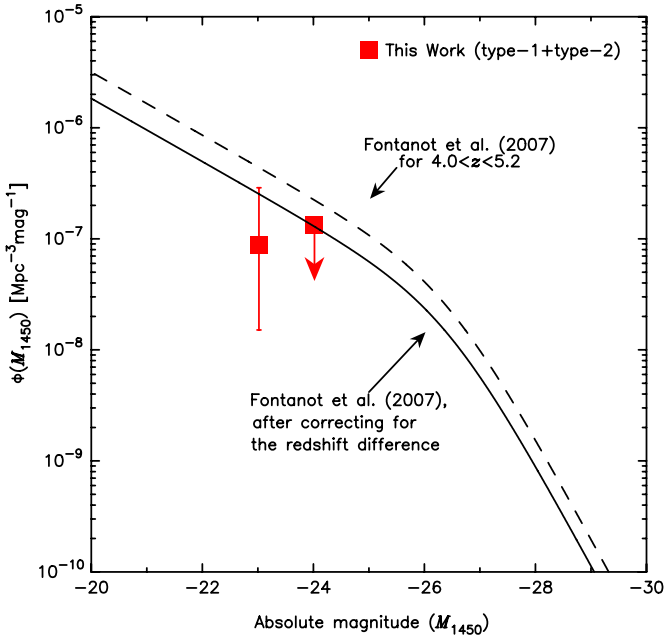

Figure 7. Comparison of $z \sim 5$ quasar luminosity functions when we include a type-2 quasar at $z \sim 5.07$. The red squares show our results when we include a type-2 quasar at $z \sim 5.07$. The black dashed and solid lines are the QLF reported by Fontanot et al. (2007), before and after correcting for the redshift difference between their study and ours (assuming pure density evolution, see the main text for details).

(A color version of this figure is available in the online journal.)

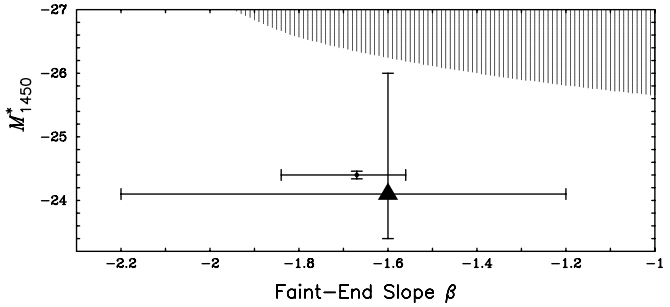

Figure 8. Constraints on the faint-end slope β and the break magnitude M^*_{1450}. The shaded region shows the parameter space that is consistent with the inferred 1σ confidence upper limits on the quasar space density at $z \sim 5$ derived in our study. A dot and triangle are the results inferred at $z \sim 4$ by Ikeda et al. (2011) and Glikman et al. (2011), respectively. Note that we estimate the errors of M^*_{1450} and the faint-end slope by applying a weighted least-squares method, while Glikman et al. (2011) estimated them by applying the STY maximum-likelihood method (Efstathiou et al. 1988).

(2007) and of ours. However, the redshift difference between the two studies should be taken into account for such a comparison because the quasar space density shows significant redshift evolution.

In Figure 7, we plot the QLF reported by Fontanot et al. (2007) after correcting for the redshift difference (i.e., taking the redshift evolution in the QLF into account), adopting model 13a in Fontanot et al. (2007). Model 13a assumes a pure density evolution of the QLF with an exponential form that gives the minimum χ^2 among the models examined in Fontanot et al. (2007). More specifically, in model 13a, the bright-end slope is fixed to be 3.31 and there are three free parameters: the faint-end slope, normalization, and redshift evolution. Figure 7 shows that our quasar space density at $z \sim 5$ is higher than the result of Fontanot et al. (2007) and thus our results are not contradictory to their result, once the redshift difference is corrected. Here it should be mentioned that Fontanot et al. (2007) adopted a different method in deriving the photometric completeness from other surveys that may introduce a possible systematic difference from other studies (see also Glikman et al. 2010). This effect is seen in Figure 6, where the inferred bright-end quasar space density is different between the results by Fontanot et al. (2007) and by Richards et al. (2006) even though the same SDSS quasar sample is used in the two studies. This suggests that the completeness adopted in Fontanot et al. (2007) may be underestimated, and accordingly the quasar space density is possibly overestimated by a factor of ∼2–3. In the case that we derive the faint end of the QLF at $z \sim 5$ by using the completeness which is calculated by Richards et al. (2006), the QLF of Fontanot et al. (2007) shifts toward lower space density in Figure 7, i.e., well below our upper limits.

In order to constrain the faint end of the QLF at $z \sim 5$ quantitatively, we search for parameter values that satisfy our result. Here we adopt the following double power-law function:

$$\Phi(M_{1450}, z) = \frac{\Phi(M^*_{1450})}{10^{0.4(\alpha+1)(M_{1450}-M^*_{1450})} + 10^{0.4(\beta+1)(M_{1450}-M^*_{1450})}}, \quad (8)$$

where α, β, $\Phi(M^*_{1450})$, and M^*_{1450} are the bright-end slope, the faint-end slope, the normalization of the luminosity function, and the characteristic absolute magnitude, respectively. Among the four parameters, the bright-end slope (α) is fixed to be $\alpha = -3.31$ based on the SDSS results (see Fontanot et al. 2007). The parameter ranges that satisfy our results are shown in Figure 8. Note that it is important to examine the redshift evolution of the faint-end slope and break magnitude because such parameters give us useful constraints on the evolutionary model of SMBHs and quasars (e.g., Hopkins et al. 2006, 2007). By taking into account the results obtained in COSMOS for

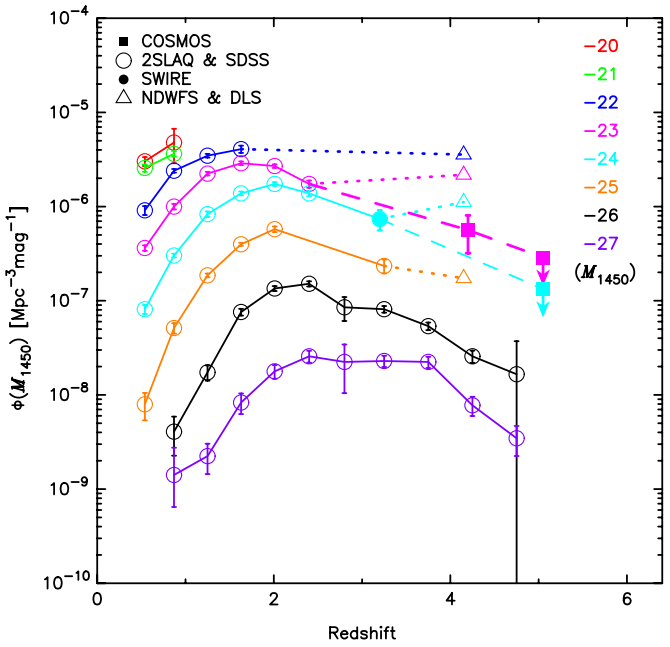

Figure 9. Redshift evolution of the quasar space density. Red, green, blue, magenta, light blue, orange, black, and purple lines are the space density of quasars with $M_{1450} = -20, -21, -22, -23, -24, -25, -26$, and -27, respectively. Filled squares, open circles, filled circle, and open triangles denote the results of different quasar surveys, as described in the upper-left side of the panel (see the main text for details). For comparison, the results of COSMOS and previous surveys are connected by the dashed lines while the results of NDWFS and DLS (Glikman et al. 2011) are connected by the dotted lines.

(A color version of this figure is available in the online journal.)

$z \sim 5$, the break magnitude in the QLF is brighter than $M^*_{1450} \sim -26$ at $z \sim 5$. This is significantly brighter than the QLF break magnitude for $z \sim 4$ reported by Ikeda et al. (2011) and Glikman et al. (2011), as shown in Figure 8. A possible explanation for this evolution is that the mass accretion in most quasars at $z \sim 5$ is higher than at $z \sim 4$ (although the quasar number density is lower at $z \sim 5$), which makes the characteristic magnitude brighter at $z \sim 5$ than at $z \sim 4$.

Here we discuss the evolution of the quasar space density in the context of the AGN downsizing. The evolution of the quasar space density for different absolute magnitude bins provides important information to constrain the evolution of SMBHs. Therefore, we plot the quasar space density for different absolute magnitude bins as a function of redshift in Figure 9. Although there are a number of low-luminosity quasar surveys at $z \sim 3$ (Wolf et al. 2003; Hunt et al. 2004; Fontanot et al. 2007; Bongiorno et al. 2007), we plot only the results of the 2dF-SDSS LRG and Quasar Survey (2SLAQ; Croom et al. 2009), the Spitzer Wide-area Infrared Extragalactic Legacy Survey (SWIRE; Siana et al. 2008), and SDSS (Richards et al. 2006), in order to avoid data with large statistical errors. While most studies at $z < 3$ suggest consistent results (i.e., the AGN downsizing), the situation is rather controversial at $z > 3$. Recently, the new $z \sim 4$ QLF results of the NOAO Deep Wide-Field Survey (NDWFS) and the Deep Lens Survey (DLS) are reported by Glikman et al. (2011). Interestingly, the results of Glikman et al. (2011) suggest constant or higher number densities of low-luminosity QSOs at $z > 3$, while our COSMOS result suggests a continuous decrease of these objects from $z \sim 2$ to $z \sim 5$.

Our result is consistent with the downsizing AGN evolution suggested by previous quasar surveys at lower z both in the optical and X-ray (e.g., Croom et al. 2009; Ueda et al. 2003; Hasinger et al. 2005). Willott et al. (2010) reported the faint end of the QLF at $z \sim 6$, although there is a large error bar for the faintest magnitude bin because only one quasar was found. The $z \sim 6$ space density at $M_{1450} \sim -22$ is lower than the upper limit of our $z \sim 5$ space density at the same magnitude and this result is also consistent with the AGN downsizing evolution. However, the results of Glikman et al. (2011) require a different picture at $z > 3$, being inconsistent with the downsizing scenario. It is not obvious what is causing this discrepancy. Masters et al. (2012) stated that cosmic variance cannot be responsible for the observed discrepancy in space density of low-luminosity quasars between the COSMOS and the DLS and NDWFS fields. If this discrepancy is due to the difference in the quasar-selection criteria, then this discrepancy could be caused by the presence or absence of the point-source selection on the *HST* images. However, both Ikeda et al. (2011) and Glikman et al. (2011) obtained the spectra of most quasar candidates to remove the contaminations. Consequently, we cannot explain this discrepancy due to the difference of the quasar-selection criteria. Therefore, it remains important that we search for low-luminosity quasars at high redshift in other fields and derive the faint end of the QLF. We also plot the quasar space density measured in the GOODS fields (Fontanot et al. 2007) in Figure 9, which is consistent with both results from Glikman et al. (2011) and COSMOS due to its large uncertainty. Further observations of low-luminosity quasars in a wider survey area are crucial to derive firm constraints on the scenarios of the quasar evolution, especially at $z > 4$.

6. SUMMARY

In order to examine the faint end of the QLF at $z \sim 5$, we select photometric candidates of quasars at $z \sim 5$ in the COSMOS field. The main results of this study are as follows.

1. Although we discover the type-2 quasar at $z \sim 5.07$, no type-1 quasars at $z \sim 5$ are identified through the follow-up spectroscopic observation.
2. The upper limits on the type-1 quasar space density are $\Phi < 1.33 \times 10^{-7}\,\mathrm{Mpc^{-3}\,mag^{-1}}$ for $-24.52 < M_{1450} < -23.52$ and $\Phi < 2.88 \times 10^{-7}\,\mathrm{Mpc^{-3}\,mag^{-1}}$ for $-23.52 < M_{1450} < -22.52$.
3. The quasar space density and its error when we include a type-2 quasar at $z \sim 5.07$ are $\Phi = 0.87^{+2.01}_{-0.72} \times 10^{-7}\,\mathrm{Mpc^{-3}\,mag^{-1}}$ for $-23.52 < M_{1450} < -22.52$.
4. The derived upper limits on the quasar space density are consistent with the QLF inferred by the previous works at $z \sim 5$.
5. The characteristic absolute magnitude of the QLF shows a significant redshift evolution between $z \sim 4$ ($M^*_{1450} > -26$) and $z \sim 5$ ($M^*_{1450} < -26$).
6. A continuous decrease of the space density of low-luminosity ($-24 \lesssim M_{1450} \lesssim -23$) quasars is inferred that is roughly consistent with the picture of the AGN downsizing evolution.

We thank the Subaru staff for their invaluable help and all members of the COSMOS team. This work was financially supported in part by the Japan Society for the Promotion of Science (JSPS; grant Nos. 23244031 and 23654068). This work was also partly supported by the FIRST program "Subaru Measurements of Images and Redshifts (SuMIRe)," which was initiated by the Council for Science and Technology Policy

(CSTP). K.M. is financially supported by the JSPS through the JSPS Research Fellowship.

REFERENCES

Bennert, V. N., Auger, M. W., Treu, T., Woo, J.-H., & Malkan, M. A. 2011, ApJ, 742, 107
Bennert, V. N., Treu, T., Woo, J.-H., et al. 2010, ApJ, 708, 1507
Bertin, E., & Arnouts, S. 1996, A&AS, 117, 393
Bongiorno, A., Zamorani, G., Gavignaud, I., et al. 2007, A&A, 472, 443
Boulade, O., Charlot, X., Abbon, P., et al. 2003, Proc. SPIE, 4841, 72
Boyle, B. J., Shanks, T., & Peterson, B. A. 1988, MNRAS, 235, 935
Brusa, M., Comastri, A., Gilli, R., et al. 2009, ApJ, 693, 8
Capak, P., Aussel, H., Ajiki, M., et al. 2007, ApJS, 172, 99
Civano, F., Brusa, M., Comastri, A., et al. 2011, ApJ, 741, 91
Civano, F., Elvis, M., Brusa, M., et al. 2012, ApJS, 201, 30
Cool, R. J., Kochanek, C. S., Eisenstein, D. J., et al. 2006, AJ, 132, 823
Croom, S. M., Richards, G. T., Shanks, T., et al. 2009, MNRAS, 399, 1755
Efstathiou, G., Ellis, R. S., & Peterson, B. A. 1988, MNRAS, 232, 431
Elvis, M., Civano, F., Vignali, C., et al. 2009, ApJS, 184, 158
Enoki, M., Nagashima, M., & Gouda, N. 2003, PASJ, 55, 133
Fan, X. 1999, AJ, 117, 2528
Fan, X., Strauss, M. A., Richards, G. T., et al. 2006, AJ, 131, 1203
Fanidakis, N., Baugh, C. M., Benson, A. J., et al. 2012, MNRAS, 419, 2797
Fontanot, F., Cristiani, S., Monaco, P., et al. 2007, A&A, 461, 39
Francis, P. J. 1996, PASA, 13, 212
Gehrels, N. 1986, ApJ, 303, 336
Glikman, E., Bogosavljević, M., Djorgovski, S. G., et al. 2010, ApJ, 710, 1498
Glikman, E., Djorgovski, S. G., Stern, D., et al. 2011, ApJ, 728, L26
Goto, T. 2006, MNRAS, 371, 769
Gültekin, K., Richstone, D. O., Gebhardt, K., et al. 2009, ApJ, 698, 198
Häring, N., & Rix, H.-W. 2004, ApJ, 604, L89
Hasinger, G., Miyaji, T., & Schmidt, M. 2005, A&A, 441, 417
Hopkins, P. F., Hernquist, L., Cox, T. J., et al. 2006, ApJ, 639, 700
Hopkins, P. F., Richards, G. T., & Hernquist, L. 2007, ApJ, 654, 731
Hunt, M. P., Steidel, C. C., Adelberger, K. L., & Shapley, A. E. 2004, ApJ, 605, 625
Ikeda, H., Nagao, T., Matsuoka, K., et al. 2011, ApJ, 728, L25
Ilbert, O., Capak, P., Salvato, M., et al. 2009, ApJ, 690, 1236
Jiang, L., Fan, X., Annis, J., et al. 2008, AJ, 135, 1057
Jiang, L., Fan, X., Bian, F., et al. 2009, AJ, 138, 305
Kashikawa, N., Aoki, K., Asai, R., et al. 2002, PASJ, 54, 819
Kawara, K., Murayama, T., Taniguchi, Y., & Arimoto, N. 1996, ApJ, 470, L85
Koekemoer, A. M., Aussel, H., Calzetti, D., et al. 2007, ApJS, 172, 196
Lawrence, A., Warren, S. J., Almaini, O., et al. 2007, MNRAS, 379, 1599
Leauthaud, A., Massey, R., Kneib, J.-P., et al. 2007, ApJS, 172, 219
Madau, P. 1995, ApJ, 441, 18
Mahabal, A., Stern, D., Bogosavljević, M., Djorgovski, S. G., & Thompson, D. 2005, ApJ, 634, L9
Marconi, A., & Hunt, L. K. 2003, ApJ, 589, L21
Masters, D., Capak, P., Salvato, M., et al. 2012, ApJ, 755, 169
McLeod, K. K., & Bechtold, J. 2009, ApJ, 704, 415
McLeod, K. K., & McLeod, B. A. 2001, ApJ, 546, 782
Merloni, A., Bongiorno, A., Bolzonella, M., et al. 2010, ApJ, 708, 137
Miyazaki, S., Komiyama, Y., Sekiguchi, M., et al. 2002, PASJ, 54, 833
Mortlock, D. J., Warren, S. J., Venemans, B. P., et al. 2011, Nature, 474, 616
Pei, Y. C. 1995, ApJ, 438, 623
Pickles, A. J. 1998, PASP, 110, 863
Richards, G. T., Strauss, M. A., Fan, X., et al. 2006, AJ, 131, 2766
Scoville, N., Aussel, H., Brusa, M., et al. 2007, ApJS, 172, 1
Siana, B., Polletta, M. d. C., Smith, H. E., et al. 2008, ApJ, 675, 49
Taniguchi, Y., Scoville, N., Murayama, T., et al. 2007, ApJS, 172, 9
Targett, T. A., Dunlop, J. S., & McLure, R. J. 2012, MNRAS, 420, 3621
Treu, T., Koopmans, L. V., Bolton, A. S., Burles, S., & Moustakas, L. A. 2006, ApJ, 640, 662
Trump, J. R., Impey, C. D., Kelly, B. C., et al. 2009, ApJ, 700, 49
Trump, J. R., Impey, C. D., Kelly, B. C., et al. 2011, ApJ, 733, 60
Ueda, Y., Akiyama, M., Ohta, K., & Miyaji, T. 2003, ApJ, 598, 886
Vanden Berk, D. E., Richards, G. T., Bauer, A., et al. 2001, AJ, 122, 549
Willott, C. J., Delorme, P., Omont, A., et al. 2007, AJ, 134, 2435
Willott, C. J., Delorme, P., Reylé, C., et al. 2009, AJ, 137, 3541
Willott, C. J., Delorme, P., Reylé, C., et al. 2010, AJ, 139, 906
Wolf, C., Wisotzki, L., Borch, A., et al. 2003, A&A, 408, 499
Woo, J.-H., Treu, T., Malkan, M. A., & Blandford, R. D. 2006, ApJ, 645, 900
Woo, J.-H., Treu, T., Malkan, M. A., & Blandford, R. D. 2008, ApJ, 681, 925